ELSEVIER

Journal of Electroanalytical Chemistry 524–525 (2002) 231–241

Journal of Electroanalytical Chemistry

www.elsevier.com/locate/jelechem

Electrosorption and catalytic properties of bare and Pt modified single crystal and nanostructured Ru surfaces

S.R. Brankovic, J.X. Wang, Y. Zhu, R. Sabatini, J. McBreen, R.R. Adžić *

Materials Science Department, Brookhaven National Laboratory, Upton, NY 11973, USA

Received 10 November 2001; received in revised form 7 December 2001; accepted 12 December 2001

Abstract

The electrosorption and catalytic properties of bare and Pt modified Ru(0001) and Ru(10 − 10) single crystal surfaces and carbon supported Ru nanoparticles have been studied by electrochemical, surface X-ray scattering, scanning tunneling microscopy, Fourier transform infrared spectroscopy and high resolution transmission electron microscopy techniques. The electrochemical surface oxidation of Ru(0001) in H_2SO_4 is an one-electron process resulting in 1 monolayer oxygen uptake and the increased spacing between the top two Ru layers from 2.13 Å at 0.1 V to 2.20 Å at 1.0 V. About 1/3 monolayer of bisulfate anions are coadsorbed with hydronium cations at low potentials. In $HClO_4$ solution, the adsorption process at ~0.1 V is due to the surface oxidation apparently to RuOH rather than to hydrogen adsorption. The oxidation of Ru(10 − 10) is quite facile and a progressive growth of the oxide layer is observed in repeated potential cycles. Spontaneous deposition of a submonolayer-to-multilayer of Pt on metallic Ru surfaces is a new phenomenon involving a noble metal deposition on a noble metal substrate through a local cell mechanism. The electrocatalysts prepared by spontaneous deposition of Pt on Ru nanoparticles have high activity and high CO tolerance exceeding those of the state-of-the-art commercial catalysts containing several times higher Pt loadings. Electronic effects appear to play a role in providing enhanced CO tolerance of Pt submonolayers on Ru nanoparticles.

Keywords: Single crystal Ru(0001) and Ru(10 − 10) electrodes; Ru oxidation; Pt deposition; Ru nanoparticles; CO tolerance

1. Introduction

The electrochemical properties of ruthenium have been the subject of extensive research because of its oxophilicity and the specific catalytic properties of oxidized Ru surfaces [1–3]. Recent activity in fuel cell development has renewed interest in Ru since it is a component of Pt–Ru catalysts for methanol and reformate H_2 oxidations [4–6]. Despite this interest, until recently, there were no data on the structural sensitivity of electrosorption properties of well-ordered Ru surfaces. A facile surface oxidation of Ru is crucial for its role as a cocatalyst in reformate H_2 and methanol oxidation. It has been conjectured that Ru provides active oxygen, so that CO can be oxidized and removed at potentials lower than those observed for Pt. Information on the structural dependence of the electrosorption and catalytic properties of Ru surfaces could help in further research into efficient Ru-based electrocatalysts. The literature contains numerous examples on the behavior of electrodeposited Ru [7–9] and bulk polycrystalline Ru samples [10], which indicate some differences in hydrogen adsorption and surface oxidation of these two materials.

Our previous studies of Ru single crystal surfaces demonstrated a pronounced role of surface structure in several reactions. For example, bisulfate was identified as adsorbed species from H_2SO_4 solutions in a wide potential region by in situ Fourier transform infrared spectroscopy (FTIR) on Ru(0001), but not on polycrystalline surfaces [11]. Carbon monoxide was found to be unusually stable on a Ru(0001) electrode surface, in sharp contrast with the facile electro-oxidation on polycrystalline surfaces. Furthermore, CO adsorbs on Ru(0001) in linear and threefold bonding configurations, while only a linear configuration has been observed on polycrystalline surfaces [12].

* Corresponding author. Fax: +1-631-344-5815.
E-mail address: adzic@bnl.gov (R.R. Adžić).

0022-0728/02/$ - see front matter © 2002 Elsevier Science B.V. All rights reserved.
PII: S0022-0728(02)00667-8

Spontaneous deposition of Pt on Ru, demonstrated recently for Pt deposition on a ultra high vacuum (UHV)-prepared Ru(0001) surface [13], represents an interesting phenomenon. This process offers a unique possibility to design the Pt–Ru electrocatalysts with desired properties and with ultimately low Pt loadings. In this article it will be illustrated by measurements of the activity of Pt submonolayers spontaneously deposited on Ru nanoparticles for the oxidation of reformate H_2. In addition, we will compare oxidation of the Ru(0001) and Ru(10 − 10) electrode surfaces, determine the structure of adsorbates on Ru(0001) in sulfuric acid solution, identify the species adsorbed on Ru(0001) in $HClO_4$ solutions and discuss some aspects of spontaneous deposition of Pt.

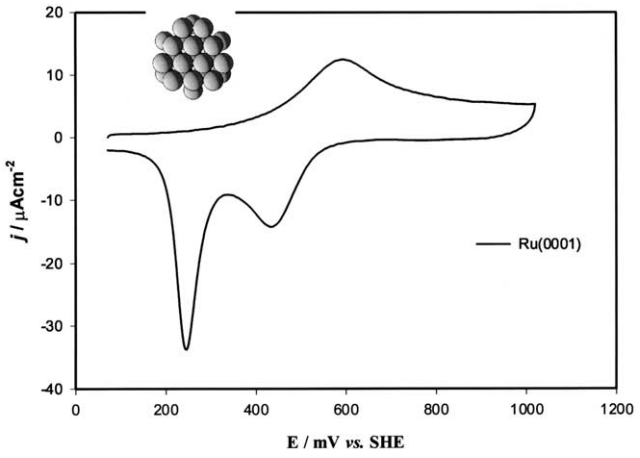

Fig. 1. Voltammetric curves of Ru(0001) in 0.1 M H_2SO_4 solution. Sweep rate 10 mV s^{-1}. Inset: a model of a Ru(0001) surface.

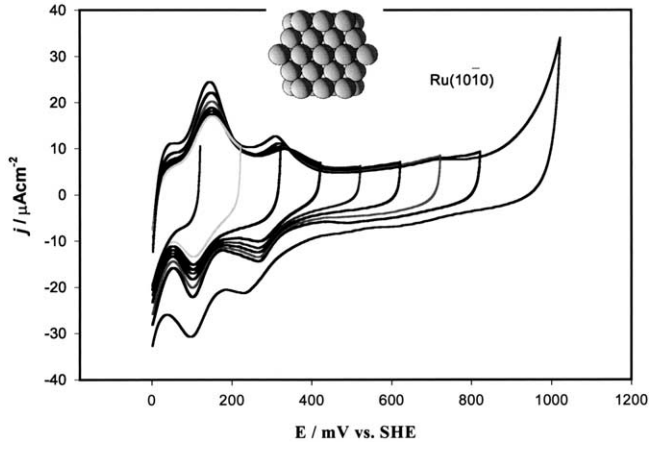

Fig. 2. Voltammetric curves of Ru(10 − 10) in 0.1 M H_2SO_4 solution. Sweep rate 10 mV s^{-1}. Inset: a model of one out of two terminations of a Ru(10 − 10) surface.

2. Experimental

The Ru(0001) and Ru(10 − 10) crystals (8 mm in diameter) were obtained from Metal Crystals and Oxides, Cambridge, England. The miscut from the (0001) and (10 − 10) faces was corrected to $< 0.1°$. The surface preparation was done in UHV following the standard procedure [14] with a final flash annealing in UHV at 1400 °C to remove the residual oxygen. After cooling in vacuum, the crystal was transferred through an Ar-filled glove box into an electrolyte solution. Protected by the solution drop or by adsorbed CO, the crystal was then mounted into an X-ray, scanning tunneling microscopy (STM) or regular electrochemical cell.

The solutions were prepared from Optima® sulfuric and perchloric acids from Fisher and MilliQC UV-Plus water (Millipore Inc.). All potentials are given with respect to a standard hydrogen electrode (SHE). STM studies were performed using a molecular imaging Pico STM with a 300S scanner and 300S Pico bipotentiostat. The cell was made of Teflon, and STM tips were prepared from 80:20 Pt–Ir wire, insulated with Apiezon wax. X-ray measurements were performed at the National Synchrotron Light Source beam line X22A with $\lambda = 1.20$ Å. Following convention, a hexagonal coordinate system was used for the Ru(0001) crystal in which the reciprocal-space wave vector was $\mathbf{Q} = Ha^* + Kcb^* + Lc^*$, where $a^* = b^* = 4\pi/\sqrt{3}a$; $a = 2.706$, $c^* = 2\pi/c$. Specular reflectivity profiles were measured with a 2×2-mm slit located 650 mm from the sample. The resulting resolution in the surface plane was 0.01 $Å^{-1}$ (full width at half maximum), which is larger than the intrinsic peak width for all measured reflections.

Transmission electron microscopy (TEM) measurements were performed by using a high-resolution 300 kV field-emission microscope (JEOL3000F) equipped with an energy filter, an energy dispersive X-ray spectrometer, and an electron energy-loss spectrometer. Powder samples mounted on Cu grids coated with carbon were used in the experiments. For quantitative analysis, all the images and diffraction patterns were recorded in either a CCD camera or an imaging plate.

3. Results and discussions

3.1. Surface oxidation of Ru(0001) and Ru(10 − 10)

3.1.1. Voltammetry curves

Figs. 1 and 2 show voltammetry curves for the surface oxidation of Ru(0001) and Ru(10 − 10) in sulfuric acid solutions. The curve for Ru(0001) in 0.1 M H_2SO_4 (Fig. 1) shows a single anodic peak and two major cathodic peaks correlated to the reduction processes. A model of the hexagonal Ru(0001) surface is

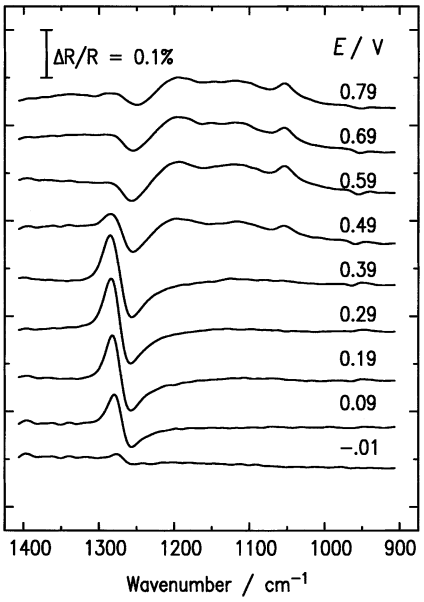

Fig. 3. In situ infrared spectra obtained from the Ru(0001) electrode in 0.05 M H_2SO_4. The reference spectrum is obtained at -0.03 V vs. SHE, and sample spectra are taken every 0.1 V, from -0.01 to 0.79 V. Scans (4096) were coadded in 16 cycles, 256 scans each; the resolution was 8 cm^{-1}. Spectra are offset for clarity.

shown as the insert in Fig. 1. The surface oxidation involves a one-electron process for which the integrated anodic charge reaches 260 $\mu C\,cm^{-2}$ in the sweep up to 1 V. Repeated potential cycling between 0 and 1.2 V did not cause significant change in the voltammetry curves. All these facts suggest that the Ru(0001) surface oxidation is limited to the top-most layer with one electron per atom exchange at the potential below the onset of bulk oxidation.

The voltammetry curve for the Ru(10 − 10) surface in 0.1 M H_2SO_4 solution (Fig. 2) shows that the oxidation of this face is more facile than that of Ru(0001), as is indicated by the onset of the oxidation at lower potentials and by increase of the charge with each potential cycle. The difference between the curves for Ru(0001) and Ru(10 − 10) surfaces suggests a high structural sensitivity of surface oxidation of Ru. A more open structure of the Ru(10 − 10) is certainly conducive to a more facile oxidation of this plane. The inset in Fig. 2 shows a model of this surface with one of the two possible terminations. The increase of the charge associated with the voltammetry curve in each subsequent cycle indicates the oxidation of several top atomic layers of this plane as observed with the polycrystalline Ru. A pair of peaks at 0.3 and 0.12 V is reminiscent of hydrogen adsorption at platinum metals. Our preliminary results show that the species associated with these peaks cannot be adsorbed hydrogen, since the charge recorded in displacing them by CO is negative rather than positive [15]. These peaks probably represent a partial Ru oxidation to RuOH (vide infra).

A similar adsorption process is observed with the Ru(0001) surface in $HClO_4$ solution (cf. Fig. 4), but not in H_2SO_4 solution [16]. This appears to be due to a strong bisulfate adsorption on a hexagonal structure of Ru(0001). Our infrared spectroscopy [11] and X-ray studies [16] show that the bisulfate adsorption on Ru(0001) is essentially at a saturation coverage between 0.0 and 0.5 V and that water chemisorbs on Ru(0001) in the absence of chemisorbed anions. Fig. 3 shows a set of spectra for anion adsorption on Ru(0001) in 0.05 M H_2SO_4, taken in 0.1 V intervals, starting from -0.01 V and ranging up to 0.79 V. A well-defined, bipolar band at $\sim 1280\ cm^{-1}$ that shifts with increasing potential is observed. The potential-dependent ν_1(ads) peak appears at around 1250 cm^{-1} for the adsorbed $(HSO_4^-)_{ad}$ species at both polycrystalline [17,18] and Pt(111) [19] surfaces. Therefore, it is quite likely that the band at 1280 cm^{-1} in Fig. 3 is due to bisulfate adsorption at Ru(0001). This high frequency, potential-dependent band can be assigned to the blue-shifted 1051 cm^{-1} absorption for bisulfate or to the sulfate-hydronium ion pair interacting with the metal surface [19]. A method for extracting unipolar bands from bipolar ones has been recently reported [11]. Strongly adsorbed bisulfate ions apparently prevent water-induced oxygen adsorption processes at low potentials and promote the complete removal of the oxygen adsorbates in the negative sweep. However, no peak for bisulfate ions in solution is visible below 0.39 V. Bipolar bands in the spectra in Fig. 3, and the lack of the solution phase band ν_1(sol) at 1051 cm^{-1}, indicate that a sizeable coverage of bisulfate is attained already at the reference potential [11].

3.1.2. Identification of adsorbed species on Ru(0001) in $HClO_4$ solutions

Identification of adsorbed species on electrode surfaces is not a simple task in particular when the species cannot be identified by some in situ spectroscopic technique. This is the situation with H, OH, or O adsorbates, and that kind of problem is encountered with the identification of the species associated with voltammetry peaks for Ru(0001) and Ru(10 − 10) surfaces. Lin et al. [20] concluded that the peak in the voltammetric curve for Ru(0001) at 0.1 V is caused by hydrogen adsorption. It would be surprising if the Ru surface was not covered by some kind of oxygen-containing species in water solutions. We have shown from X-ray scattering data [16] that in pure water Ru(0001) is covered by a full monolayer (ML) of chemisorbed H_2O (vide infra). Here we report preliminary data on the identification of adsorption processes on Ru surfaces obtained by using CO to displace the adsorbed species. Using CO to displace adsorbed species in voltammetric [21] and charged displacement [22,23] experiments has been proved useful in confirming the identity of the species

adsorbed on the Pt(111) surface. The charge displacement technique was reported by Conway and coworkers [24] by utilizing acetonitrile to elucidate the adsorption at a Pt electrode.

Fig. 4 shows the voltammetric curve obtained with Ru(0001) annealed in H_2 at 1100 °C. To identify the nature of the species adsorbed at potentials from 0 to 140 mV, the electrode was kept at a constant potential of 40 mV and CO was introduced into the cell. There is no significant CO oxidation on Ru(0001) in this potential range. The charge associated with the ensuing displacement process was measured and it is shown as the insert to Fig. 4. A negative charge of $-117\ \mu C\,cm^{-2}$ was found, which means that H_{ad} cannot be the adsorbed species in that potential region, but contrary to the conclusion of Lin et al., it is associated with some oxygen-containing species. A plausible reaction to account for this negative charge is

$$RuOH + CO_{soln} + e^- \rightarrow RuCO_{ad} + OH^- \quad (1)$$

The measurement at 0.14 V revealed again a negative, albeit a smaller charge of $-31\ \mu C\,cm^{-2}$. This indicates that some transformation of the species existing at 0.04 V took place. The difference between the charges at 0.04 and 0.14 V is 79 $\mu C\,cm^{-2}$, which is in good agreement with 86 $\mu C\,cm^{-2}$, the voltammetric charge in that potential interval. Further analysis of these processes and the data for Ru(10 − 10), which also always show a negative displacement charge, will be published at a future date.

3.1.3. Surface X-ray scattering measurements

To characterize the atomic structure of the Ru(0001) electrode as a function of potential, X-ray specular reflectivity profiles were measured at 0.1 and 1.0 V in 1 M H_2SO_4. In Fig. 5, the structure factor intensities are shown after correcting the integrated intensities for the variation of the Lorentz factor, the effective sample area, and the resolution along the surface normal direction [25]. Simulations indicate that the deep minima in Fig. 5 could result from either adsorption of species from solution phase or changes in the top layer of the substrate. The best fit (solid line) gives a 2.13 ± 0.01 Å spacing between the top two Ru layers and an RMS displacement amplitude of 0.13 ± 0.02 Å for the top Ru layer, which assumes the coadsorption of 1/3 ML of bisulfate and 1/3 ML of hydronium ion. The saturated coverage for bisulfate is expected to be about 1/3 or 0.4 ML based on its size relative to the Ru(0001) surface. Another case for sulfate/bisulfate adsorption over a

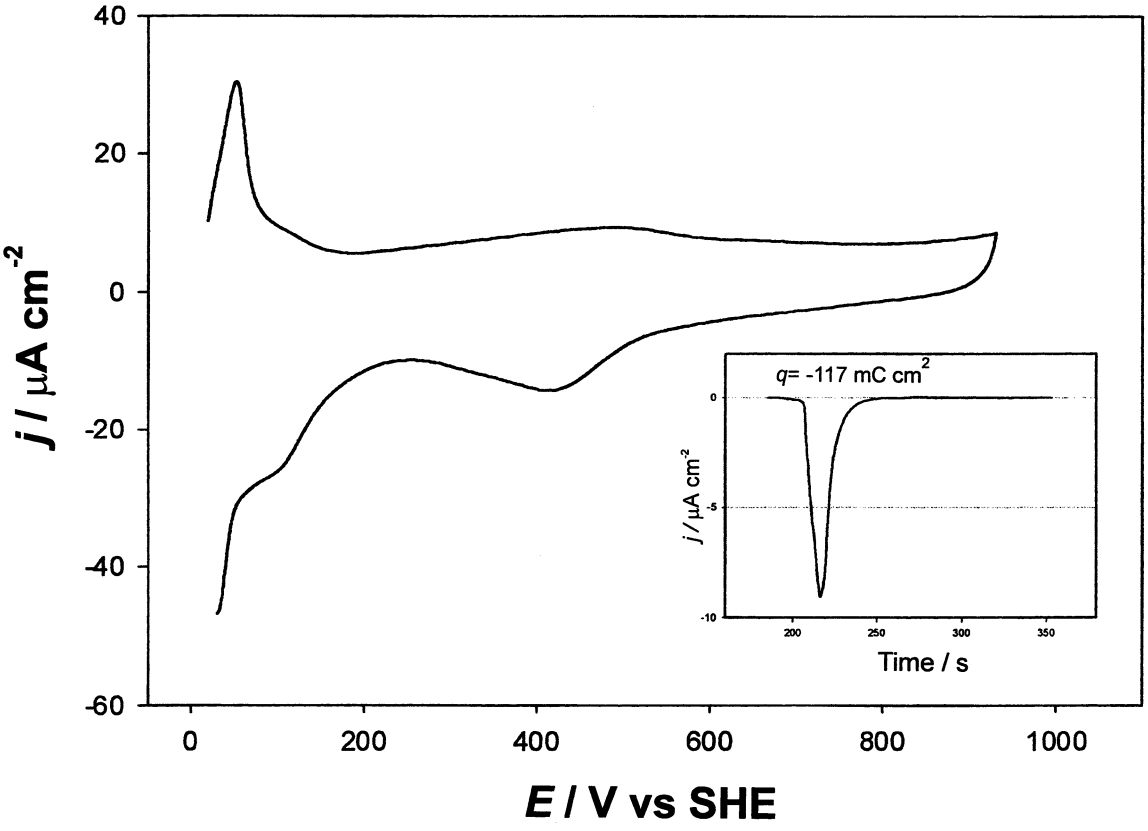

Fig. 4. Voltammetric curve for the oxidation of Ru(0001) in 0.1 M $HClO_4$ solution, sweep rate 20 mV s^{-1}. Inset shows the charge associated with the displacement of adsorbed species at 0.1 V by adsorption of CO.

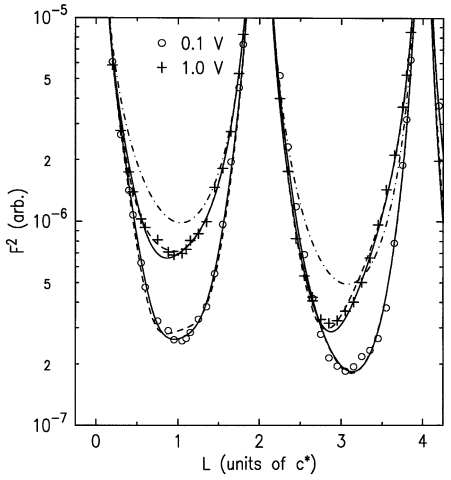

Fig. 5. Specular reflectivity (structure factor squared) measured for Ru(0001) at 0.1 V (circles) and 1.0 V (plus sign) in 1 M H_2SO_4 with the dot–dash line showing the calculated curve for an ideally terminated Ru(0001). The dashed and solid lines are the fits discussed in the text.

wide potential region has been reported for the Rh(111) surface [26]. A large bisulfate adsorption precludes the Ru(0001) surface oxidation at low potentials. The specular reflectivity measurements obtained from Ru(0001) in pure water suggests that water is strongly chemisorbed on Ru(0001) with a 2.03 ± 0.05 Ru–O layer spacing and causing a Ru layer expansion [16]. Thus, the expansion of Ru layer spacing in pure water suggests that the water adsorption involves an oxidation process, which is circumvented by the adsorption of bisulfate. In 1 M strong acid solution at low potentials, the coadsorbed oxygen species is likely to be the hydronium ion (H_3O^+). As illustrated in Fig. 6, the two adlayers are nearly coplanar. The lateral electrostatic repulsion among the bisulfate anions can be reduced by the coadsorption of H_3O^+ cations. This kind of cation–anion coadsorption usually results in a constant coverage over a range of potentials [27], and thus the high bisulfate coverage is reached at a very low potential.

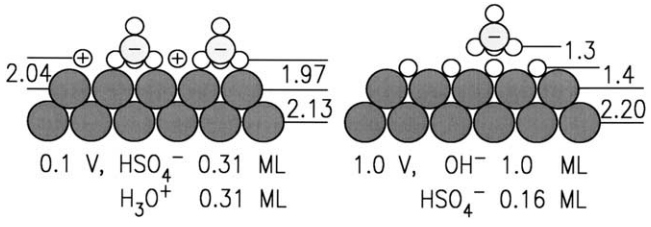

Fig. 6. Proposed schematics of structural models where the O, S, and Ru atoms are represented by the open, heavily shaded, and lightly shaded circles, respectively. The layer spacings are given in angstrom and coverages are given in monolayer (ML).

At potentials positive of the anodic current peak, a partial desorption of bisulfate has been observed by FTIR [11], which is believed to be a result of the formation of a surface oxide. This is confirmed by the analysis of the specular reflectivity obtained at 1.0 V shown by the plus symbol in Fig. 5. The clearest evidence for that is the 2.20 ± 0.02 Å spacing between the top two Ru layers, which was found to be independent of the details on the adlayer structure and similar to the value (2.22 Å) for 1 ML of oxygen on Ru(0001) in gas-phase oxidation [28]. For the oxygen and bisulfate adlayers, the fitting parameters are strongly correlated. The solid line was obtained by fitting with the spacing between the oxygen layer and the top Ru layer initially fixed at about 1 Å. This fit gives 0.8 ML of oxygen located at 1.2 Å above Ru, and 0.24 ML of bisulfate located at 0.7 Å above the oxygen layer. Fitting with the oxygen layer located under the top Ru layer failed to yield a good fit and, on this basis, we can rule out the existence of subsurface oxygen. Based on these results, a proposed structural model is shown in Fig. 6 (right side). Although the parameters given for the adsorbates (average values from two sets of parameters) have large error bars, the results do support the formation of surface oxide and suggest that a monolayer of oxygen species is chemisorbed and stays on top of the Ru(0001) surface at 1.0 V. This, in turn, results in a partial desorption of bisulfate. No place exchange mechanism in Ru(0001) oxidation is observed as it is for Pt(111) [29] and Au(111) [30,31]. On the basis of the voltammetry, X-ray scattering and FTIR spectroscopy data we can write the following equation for the surface oxidation of Ru(0001) at $E >$ 0.40 V:

$$\mathrm{Ru} + \mathrm{H_2O} \rightarrow \mathrm{RuOH} + \mathrm{H^+} + \mathrm{e^-} \quad (2)$$

No ordered oxygen adlayers have been identified on Ru(0001) in sulfuric acid solutions from in-plane diffraction features, which have been obtained in UHV by low-energy electron diffraction (LEED) and Auger electron spectroscopy (AES) on the Ru(0001) electrode emersed from 0.1 M $HClO_4$ solution [20]. It is difficult to rule out the existence of ordered structures in in situ measurements since the expected X-ray intensity from an oxygen adlayer is weak relative to the diffuse scattering background. However, there is also no indirect evidence to support these submonolayer oxygen phases in sulfuric acid from the specular reflectivity measurements. Nevertheless, both the in situ X-ray and ex situ LEED and AES studies show that the initial state of Ru(0001) oxidation involves oxygen adsorption of up to 1 full monolayer at potentials below the onset of Ru bulk oxidation in acid solutions. The structural phase behavior of Ru surface oxidation is distinctly different from those observed for other noble metal surfaces.

3.2. Spontaneous deposition of Pt on Ru single crystals and nanoparticles

3.2.1. Pt submonolayer-to-multilayer deposition on Ru(0001)

Spontaneous deposition of Pt on Ru [13] is an unusual phenomenon, since it involves a monolayer-to-multilayer deposition of one noble metal (Pt) on another noble metal (Ru). The spontaneous deposition of Pt on Ru(0001) has been demonstrated for Ru(0001) immersed in 10^{-2} or 10^{-4} M $[PtCl_6]^{2-} + 0.1$ M H_2SO_4 solutions. The Ru crystal was immersed in the platinum-containing solution immediately after the transfer from the UHV chamber to an Ar filled glove box. The STM images shown in Fig. 7 were recorded in 0.1 M H_2SO_4 solution at a potential of 0.370 V. The morphology of a Pt deposit on a single Ru crystal immersed in a 10^{-4} M $PtCl_6^{2-} + 0.1$ M H_2SO_4 solution for 2 min is presented in Fig. 7A. One can see that the Ru surface is decorated with a great number of Pt nanoparticles. The Pt nanoparticles have a columnar shape and relatively uniform size. Their height is in the range of 3–5 nm (10–15 MLs and their diameter is between 6 and 10 nm (Fig. 7A). The clusters cover about 35% of the Ru surface, as determined from the STM images. By assuming the average height of the clusters to be 4 nm ($\sim$ 13 ML), one can estimate that the total amount of Pt deposited is between 4 and 5 ML.

A representative STM image of a Pt deposit obtained by immersing a freshly prepared Ru single crystal in the 10^{-2} M $PtCl_6^{2-} + 0.1$ M H_2SO_4 solution for 1 min (half of the time for the deposit in Fig. 7A) is shown in Fig. 7B. The entire Ru surface is covered with 2–6 nm-sized Pt clusters. There is an indication of a slight preferential deposition of Pt on step edges. The average height of the Pt clusters deposited on the Ru terraces is 2 ML, while the clusters that are deposited along the step edges are in general 1 ML higher (3 ML). Fig. 7A and B show that, depending on the experimental conditions, Pt deposits of vastly different morphologies can be obtained on Ru(0001) surfaces.

'Spontaneous' or 'irreversible' adsorption was observed quite some time ago for non-noble metal cations on noble metal substrates. This deposition was accomplished by immersion of clean noble metal surfaces in cation-containing solutions, which produces adlayers strongly interacting with the substrate without the application of an external potential [32,33]. Spontaneous adsorption also occurs when the noble metal is immersed in a noble metal ion containing solution, as was recently shown by Wieckowski and coworkers for the deposition of Ru adlayers on a Pt(*hkl*) surface [34,35]. Submonolayer amounts of metal were deposited apparently through irreversible anion adsorption, since an additional voltammetric treatment was necessary to obtain metallic deposits. The maximum coverage of Pt electrode by the Ru deposit was reported to be not higher than 20% as inferred from the AES and STM measurements [36]. These surfaces showed considerable catalytic activity for the methanol oxidation reaction [34,35,37]. Spontaneous deposition was also reported for Pd on polycrystalline [32] and single crystal Pt electrodes [38–40]. A Pd deposit of up to a ML was found in Ref. [38], while the amount of deposited Pd in the second case was considerably lower. Only forced deposition using H_2 as a reducing agent resulted in deposits of higher coverages [39]. This analysis indicates that the spontaneous deposition of Pt on the Ru(0001) surface forming monolayer-to-multilayer deposits is a different phenomenon from the spontaneous deposition of Ru or Pd on Pt reported for the Ru–Pt(*hkl*) [34,35] and Pd on Pt(111) [38,39] systems.

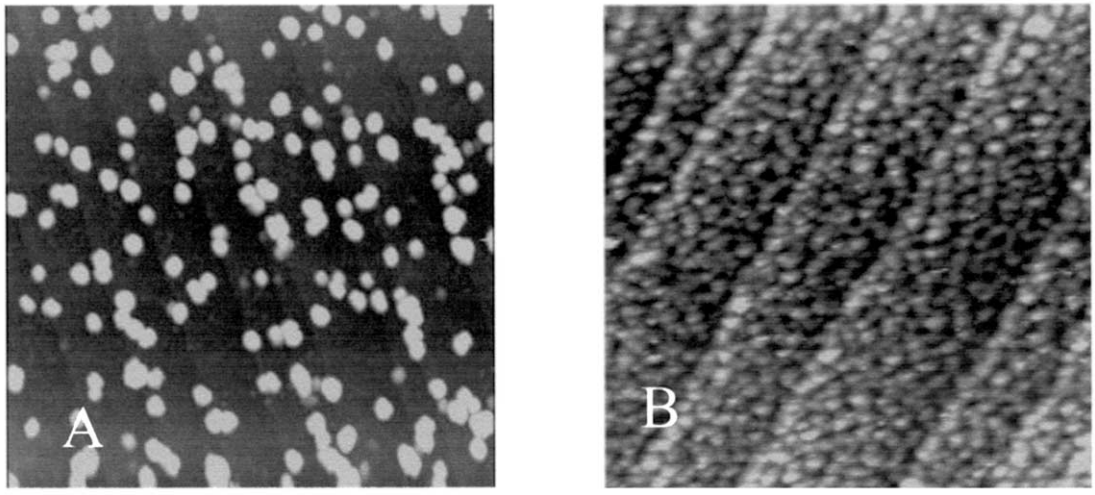

Fig. 7. STM images in H_2SO_4 solution of: (A) Pt clusters spontaneously deposited on Ru(0001) in 0.1 mM $H_2PtCl_6 + 0.1$ M H_2SO_4 solution (see text for details); (B) Pt adlayer spontaneously deposited on Ru(0001) in 10 mM $H_2PtCl_6 + 0.1$ M H_2SO_4 solution (see text for details). Image A: 200×200 nm, Z range 5 nm; image B: 100×100 nm, Z range 2 nm. Images recorded at open circuit potential in 0.1 M H_2SO_4.

A comparison of the above STM data with the STM data for a spontaneously deposited submonolayer of Ru on Pt(111) [36,41–44] and electrodeposited Ru on Pt(111) [45] shows that more uniform deposits and a smaller tendency towards a three-dimensional (3D) growth can be expected for Pt on Ru deposition. It is interesting that in the case of spontaneous deposition of Pd on Ru(0001) an atomically ordered pseudomorphic Pd layer was observed [46].

Spontaneous deposition of Pt on Ru(0001) requires a metallic, freshly prepared surface; it does not occur on surfaces oxidized in contact with acids or even water. The driving force for this process could be the difference between the potential of $PtCl_6^{2-}$ reduction (onset of Pt deposition), and the potential of Ru^0 oxidation [13]. It is, however, not clear to what extent the Ru oxidation reaction takes place in a spontaneous multilayer deposition of Pt. The fact that Pt can form a multilayer deposit on a Ru surface indicates that, either the oxidation of Ru to Ru(OH) is not limited to strictly one (surface) monolayer, or a higher oxidation state of Ru is formed, or some third reaction is taking place. The oxidative dissolution of Ru can be excluded because it occurs at potentials more positive than the equilibrium potential of $Pt/PtCl_6^{2-}$. A Ru(0001) oxidation to RuOH in non-adsorbing acid solutions occurs at $E = 0.3$ V, which is more negative than the equilibrium potential of $Pt/PtCl_6^{2-}$, and the condition for Pt spontaneous deposition is satisfied. In situ SXS and voltammetry of the oxidation of Ru(0001), however, show that the oxidation beyond a monolayer of RuOH requires very high potentials above 1.2 V. Its dissolution is unlikely since it cannot be dissolved even in aqua regia. Therefore, further work is needed to clarify this mechanism for single crystal surfaces. In the case of spontaneous deposition of Pt on carbon supported Ru nanoparticles described below, certain dissolution of Ru was clearly identified. The AES analysis of the deposit obtained from the solution remaining after spontaneous deposition of Pt clearly showed the presence of Ru. Ru nanoparticles are more reactive than the hexagonal Ru(0001) surface, which can explain some dissolution of Ru observed with them.

3.2.2. Electrocatalytic properties of Pt submonolayers on Ru nanoparticles

The approach developed in the study of spontaneous deposition of Pt on Ru(0001) was used to deposit Pt on Ru nanoparticles on a carbon substrate. It was found that spontaneous deposition of Pt also occurs on the Ru nanoparticles reduced in H_2 at elevated temperatures. This opens the possibility of decorating the surface of Ru nanoparticles with 2D Pt clusters and thus of 'tailoring' the properties of the Pt–Ru bimetallic electrocatalysts on an atomic level. In addition, this approach facilitates a considerable reduction of Pt loadings by depositing Pt only at the surface of Ru nanoparticles rather than having Pt throughout the Pt–Ru nanoparticles. In contrast to the Pt–Ru alloy catalysts, this structure has most of the Pt atoms available for the catalytic reaction. The properties of the new Pt–Ru catalyst prepared in this way are tested and its activity compared with that of the commercial Pt–Ru alloy catalysts with the same nanoparticle size.

Preparation of this Pt–Ru electrocatalyst involved treatment of Ru (10%) nanoparticles on Vulcan XC-72 carbon in an H_2 atmosphere at ~ 300 °C for 2 h. After cooling down to the room temperature, they were immersed in a solution of $PtCl_6^{2-}$ ions. The entire procedure was carried out in either an H_2 or an Ar atmosphere and the amount of Pt available for spontaneous deposition was controlled by the concentration and volume of the immersing solution. The modified nanoparticles were dispersed in a 100 ml of ultrapure water and sonicated for 30 min. Aliquots (several μl) of sonicated dispersion of Pt modified Ru nanoparticles were applied to glassy carbon rotating disk electrodes and covered by very thin (1–3 nm) Nafion® films [47,48].

A considerable amount of work has been done in the characterization of carbon supported metal nanoparticles. A prevailing view is that they are in the form of cubo-octahedral [49] and icosohedral [50] structures. A model of a cubo-octahedral Ru nanoparticle with a 1/4 ML of Pt and a possible distribution of Pt clusters is given in Fig. 8. We use the Ru nanoparticle as a reducing agent to serve as a core of the Pt–Ru catalyst nanoparticles. Pt is expected to cover the Ru surface as 2D islands, as long as a small coverage of Pt is deposited by using a relatively high H_2PtCl_6 concentration as was done to obtain the deposit in Fig. 7B.

The catalyst prepared by spontaneous deposition of Pt on Ru(10% wt)/Vulcan XC 72 (E-TEK) was examined by high resolution TEM. A sample of 0.1 g Ru–C (10% wt.) which contained 100 μmol Ru atoms was immersed in 5 ml of 1 mM H_2PtCl_6 solution (5 μmol Pt ions) after it had been heated at 300 °C under a hydrogen flow for 2 h and then cooled down to room temperature. The Pt–Ru atomic ratio in the sample was thus 1:20. Because of the small amount of Pt relative to Ru, no attempt has been made to determine the location of Pt atoms by using TEM chemical and diffraction analyses in the present study. Fig. 9a shows a typical morphology of the metal nanoparticles on the carbon support. The dark spotty contrast in the image represents the nanoparticles of heavy metal atoms located at the surface of the spherical carbon balls that have an average size of about 50 nm. Measurements of over a hundred metal particles from TEM images yield an average diameter about 2.5 nm, slightly larger than the value (2 nm) for as received Ru–C sample according to the E-TEK specification. Clearly, there is no

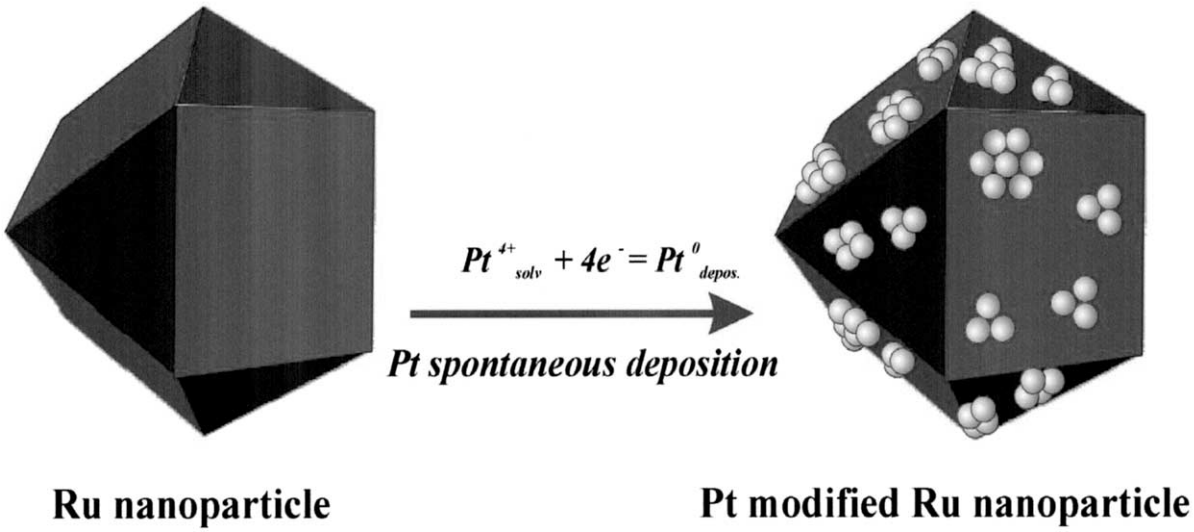

Fig. 8. Model of a cubo-octahedral Ru nanoparticle covered by 1/4 of a Pt monolayer.

significant aggregation due to the heating and Pt deposition.

Fig. 9b–d shows high-resolution images of the nanoparticles with 1D and 2D lattices. To identify the crystal structure of the particles, diffraction analysis was carried out on about 170 particles using a special computer routine based on fast Fourier transform of the lattice images of the particles. We found that the dominant features observed, both in symmetry and lattice spacing, are consistent with the hexagonally close-packed (hcp) Ru single crystal structure. An example is shown in Fig. 9e with the angles and lattice constants marked for the low-index reflections. The diffractogram (Fig. 9e) was Fourier transferred from the boxed area in Fig. 9d where the particle is viewed along the (-101) direction.

Fig. 10 plots the distribution of the observed lattice spacing of the nanoparticles. The most frequently observed lattice fringes fit well with the hcp Ru single crystal structure. A small amount of RuO_2 is likely to exist because the observed lattice spacing around 0.225 nm can be best explained by the (002) lattice constant of the body centered tetragonal structure of RuO_2.

Fig. 11 displays a comparison of the current densities at $E = 0.05$ V as a function of time recorded with a rotating disk thin film electrode at 2500 rpm for the oxidation of H_2 and H_2 with 100 ppm of CO for the electrocatalysts $Pt–Ru_{20}$ obtained by spontaneous deposition, and for the E-TEK's Pt–Ru alloy catalyst. The catalyst loadings are calculated with respect to the total amount of Pt and they were 0.95 and 2.93 $\mu g\,cm^{-1}$, respectively. The time dependence of the normalized current density at 50 mV shows a considerably better CO tolerance of the electrocatalyst obtained by spontaneous deposition despite the three times lower Pt amount, as demonstrated in a recent note [51]. The

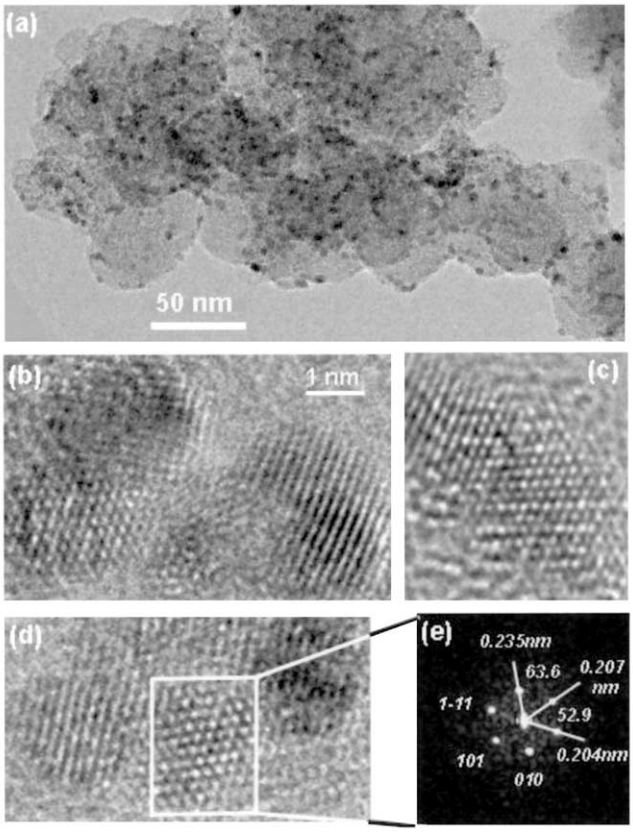

Fig. 9. Electron micrographs of Ru nanoparticles. (a) Low magnification morphology of the particles (black dots) on carbon spheres. (b–d) High-resolution images of the particles which have an average diameter of about 2.5 nm. (e) Diffractogram obtained from the high-resolution image shown in (d) (boxed area). Diffraction analysis reveals that the angles and lattice constants are consistent with the hcp Ru single crystal structure.

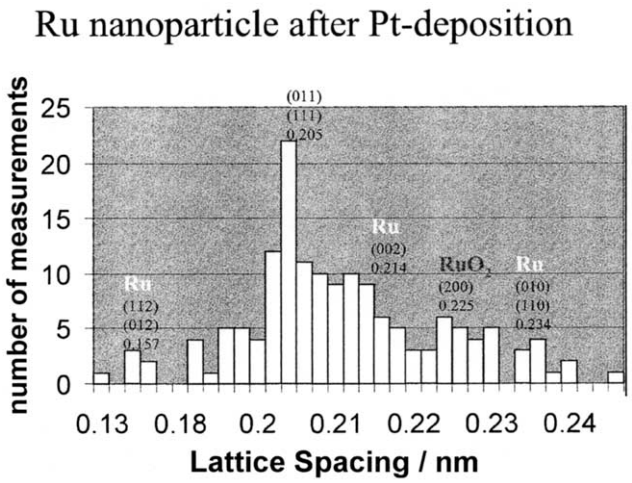

Fig. 10. Lattice spacing distribution of the nanoparticles measured from the high-resolution images (~ 170 measurements) showing that the particles are mainly metallic Ru with a small amount of RuO_2.

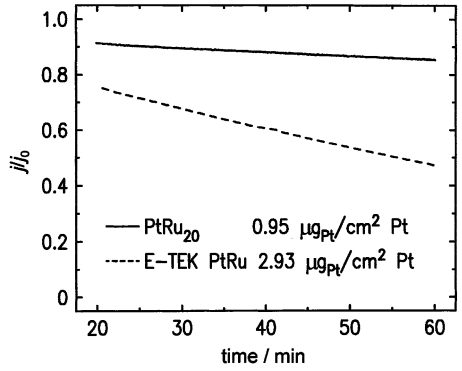

Fig. 11. Time dependence of the normalized current densities at $E = 0.05$ V for the oxidation of H_2 and H_2 with 100 ppm CO in 0.5 M H_2SO_4 at 25 °C obtained by using a thin-film rotating electrode at 2500 rpm for the electrocatalyst prepared by spontaneous deposition of a submonolayer Pt on Ru containing 0.95 μg cm^{-2} of Pt, and for E-TEK's 1:1 Pt–Ru alloy catalyst containing 2.93 μg cm^{-2} of Pt; j_o is the H_2 oxidation current density. During the first 20 min the current fluctuations (not shown) are large due to a conditioning of the solution.

current density for the oxidation of the pure H_2 is used for normalization, as it is the same for both electrocatalysts. During the first 20 min, not shown in the graph, a $H_2 + CO$ mixture was bubbled through the solution while the electrodes were subjected to the same polarization and rotation regimes as indicated in the figure. The curves in Fig. 11 represent typical results. Most recently, spontaneous deposition of Ru on Pt nanoparticles [52] has been used to prepare active catalysts for CH_3OH oxidation. It remains to be seen whether spontaneous deposition of Pt on Ru nanoparticles can produce similar methanol oxidation electrocatalysts with submonolayer Pt loadings.

The higher CO tolerance of the spontaneously deposited Pt on Ru than that of the Pt–Ru alloy electrocatalyst is likely to be a consequence of the electronic effect with some role for the bifunctional mechanism. The latter has often been cited for the Pt–Ru system because of RuOH formation at low potentials, which helps in CO oxidation. At low overpotentials, viz. 50–100 mV, in addition to RuOH, the Ru surface is covered by strongly adsorbed H_2O, as discussed above. Both species are probably taking part in the oxidation of CO. Our in situ FTIR has shown that there are two distinct CO vibration bands on Pt–Ru(0001), while a single band is observed for Pt–Ru alloy [53]. This indicates a rather different electronic interaction between the Pt submonolayer and Ru and Pt and Ru in the alloy. Relativistic density-functional studies using a two-layer cluster model have shown that the CO adsorption energy on the Pt–Ru model is the lowest in comparison with pure Pt, pure Ru, and Pt–Ru/Pt models [54]. The temperature programmed desorption (TDS) data for CO on Pt-on Ru(0001) also indicate a decrease in bonding strength of CO to Pt [55]. Koper et al. [56] have recently reported a density functional theory (DFT) calculation, which shows that the lowest CO bonding is observed for the Pt monolayer on a Ru(0001) surface. The model of Hammer and Nørskov [57] for the binding trends of CO on modified transition-metal surfaces and alloys shows that an effective transfer of d electrons from Pt to Ru takes place and the Pt d-band shifts down in order to maintain the pure d-band filling and charge neutrality. The lowering of the d-band causes a weaker CO adsorption because of decreased back donation from Pt to antibonding CO orbitals. Both experimental and theoretical data suggest a favorable electronic effect that reduces the CO adsorption energy on the Pt submonolayer on a Ru catalyst in comparison to pure Pt and Pt–Ru bulk alloy.

4. Summary

Electrochemical properties of Ru(0001) and Ru(10 − 10) surfaces exhibit a high structure sensitivity. In acid solutions, the voltammetric curves for Ru(0001) show a one-electron surface oxidation process at potentials below the onset of bulk oxidation, which is supported by X-ray scattering data. Furthermore, the analysis of the X-ray specular reflectivity found that the spacing between the top two Ru layers is 2.13 Å at 0.1 V and 2.20 Å upon oxidation at 1.0 V in 1 M sulfuric acid solution. At low potentials, specular reflectivity data support a model involving the coadsorption of bisulfate and hydronium ions on Ru(0001). In contrast to the behavior of Pt(111) and Au(111) surfaces, no place exchange is involved in the Ru(0001) surface oxidation. On the other hand, the oxidation of Ru(10 − 10) is quite facile and a progressive growth of the oxide layer is observed in repeated potential cycles.

The spontaneous deposition of Pt on Ru(0001) is a new phenomenon involving a noble metal deposition on a noble metal substrate. A local cell mechanism appears to be responsible for Pt deposition on Ru, where Ru oxidation to RuOH is the cathodic reaction occurring on the crystal surface. The coverage and morphology of the Pt deposit can be conveniently controlled by the time of crystal immersion and concentration of $PtCl_6^{2-}$ ions. The electrocatalysts prepared by spontaneous deposition of Pt on Ru nanoparticles have high activity and high CO tolerance exceeding those of the state-of-the-art commercial catalysts containing several times higher Pt loadings. Electronic effects appear to play a role in providing enhanced CO tolerance of Pt submonolayers on Ru nanoparticles.

Acknowledgements

This work is supported by the US Department of Energy, Divisions of Chemical and Material Sciences, under Contract No. DE-AC02-98CH10886. The authors thank L. Wu for his assistance in TEM experiments and S. Feldberg for useful discussions.

References

[1] S. Trasatti, W.E. O'Grady, in: H. Gerisher, C. Tobias (Eds.), Advances in Electrochemistry and Electrochemical Engineering, vol. 12, Wiley, New York, 1982.
[2] S. Gottesfeld, T. Zawodzinski, in: D.M. Kolb, R. Alkire (Eds.), Advances in Electrochemical Science and Engineering, vol. 5, VCH, New York, 1997, p. 195.
[3] P. Ross, in: J. Lipkowski, P.N. Ross (Eds.), Electrocatalysis, Wiley–VCH, New York, 1998, p. 197.
[4] H.A. Gasteiger, N.M. Markovic, P.N. Ross, E.J. Cairns, J. Phys. Chem. 97 (1993) 12020.
[5] A. Hamnett, in: A. Wieckowski (Ed.), Interfacial Electrochemistry: Theory, Experiment and Application, Marcel Dekker, New York, 1999, p. 843.
[6] T. Iwasita, H. Hoster, A. John-Anacker, W.F. Lin, W. Vielstich, Langmuir 16 (2000) 522.
[7] S. Hadži-Jordanov, H. Angerstein-Kozlowska, M. Vuković, B.E. Conway, J. Electrochem. Soc. 125 (1978) 1569.
[8] B.E. Conway, Electrochemical Supercapacitors: Scientific Foundations and Technological Applications, Kluwer Academic/Plenum, New York, 1999.
[9] V. Horvat-Radosević, K. Kvastek, M. Vuković, D. Čukman, J. Electroanal. Chem. 482 (2000) 188.
[10] R.C. Walker, M. Baisiles, L.M. Peter, Electrochim. Acta 44 (1998) 1289.
[11] N.S. Marinković, J.X. Wang, H. Zajonz, R.R. Adžić, J. Electroanal. Chem. 500 (2001) 388.
[12] (a) N.S. Marinković, J.X. Wang, H. Zajonz, R.R. Adžić, Electrochem. Solid-State Lett. 3 (2000) 11;
(b) N.S. Marinković, H. Zajonz, R.R. Adžić, 195th Electrochem. Soc. Meeting, Book of Abstracts, Seattle, WA 1999, p. 1044.
[13] S.R. Brankovic, J. McBreen, R.R. Adžić, J. Electroanal. Chem. 503 (2001) 99.
[14] T.E. Madey, H.A. Engelhardt, D. Menzel, Surf. Sci. 48 (1975) 304.
[15] J. Clavilier, R. Albalat, R. Gomez, J.M. Orts, J.M. Feliu, A. Aldaz, J. Electroanal. Chem. 330 (1992) 489.
[16] J. Wang, N.S. Marinković, H. Zajonz, B.M. Ocko, R.R. Adžić, J. Phys. Chem. 105 (2001) 2809.
[17] H. Ogasawara, Y. Sawatari, J. Inukai, M. Ito, J. Electroanal. Chem. 358 (1993) 337.
[18] R.J. Nichols, in: J. Lipkowski, P. Ross (Eds.), Adsorption of Molecules at Metal Electrodes, VCH, New York, 1991 (Ch. 7).
[19] P.W. Faguy, N.S. Marinković, R.R. Adžić, J. Electroanal. Chem. 407 (1996) 41.
[20] W.F. Lin, M.S. Zei, Y.D. Kim, H. Over, G. Ertl, J. Phys. Chem. B 104 (2000) 6040.
[21] R.R. Adžić, F. Feddrix, E. Yeager, J. Electroanal. Chem. 341 (1992) 287.
[22] J. Feliu, J.M. Orts, R. Gómez, A. Aldaz, J. Clavilier, J. Electroanal. Chem. 372 (1994) 265.
[23] J.M. Orts, R. Gomez, J.M. Feliu, A. Aldaz, J. Clavilier, Electrochim. Acta 39 (1994) 1519.
[24] B. MacDougall, B.E. Conway, H. Angerstein-Kozlowska, J. Electroanal. Chem. 32 (1971) 477.
[25] I.K. Robinson, in: D.E. Moncton, G.S. Brown (Eds.), Handbook on Synchrotron Radiation, vol. 3, North-Holland, Amsterdam, 1991, p. 221.
[26] Y.-E. Sung, S. Thomas, A. Wieckowski, J. Phys. Chem. 99 (1995) 13513.
[27] J.X. Wang, I.K. Robinson, J.E. DeVilbiss, R.R. Adžić, J. Phys. Chem. 33 (2000) 7951.
[28] Y.D. Kim, S. Wendt, S. Schwegmann, H. Over, G. Ertl, Surf. Sci. 418 (1998) 267.
[29] H. You, D.J. Zurawski, Z. Nagy, R.M. Yonco, J. Chem. Phys. 100 (1994) 4699.
[30] C.M. Vitus, A.J. Davenport, J. Electrochem. Soc. 141 (1994) 1291.
[31] Unpublished results of X-ray scattering study.
[32] M.M.P. Jansenn, J. Moolhuysen, Electrochim. Acta 21 (1976) 861.
[33] J. Clavilier, J.M. Feliu, A. Aldaz, J. Electroanal. Chem. 243 (1988) 419.
[34] W. Chrzanowski, A. Wieckowski, Langmuir 13 (1997) 5974.
[35] W. Chrzanowski, H. Kim, A. Wieckowski, Catal. Lett. 50 (1998) 69.
[36] E. Herrero, J.M. Feliu, A. Wieckowski, Langmuir 15 (1999) 4944.
[37] G. Tremiliosi-Filho, H. Kim, W. Chrzanowski, A. Wieckowski, B. Grzybowska, P. Kulesza, J. Electroanal. Chem. 467 (1999) 143.
[38] G.A. Attard, A. Bannister, J. Electroanal. Chem. 300 (1991) 467.
[39] J. Clavilier, M.J. Llorka, J.M. Feliu, A. Aldaz, J. Electroanal. Chem. 310 (1991) 429.
[40] M.J. Llorka, J.M. Feliu, A. Aldaz, J. Clavilier, J. Electroanal. Chem. 351 (1993) 299.
[41] E. Herrero, K. Franaszczuk, A. Wieckowski, J. Electroanal. Chem. 361 (1993) 269.
[42] W. Chrzanowski, A. Wieckowski, Langmuir 13 (1997) 5974.
[43] J. Clavilier, J.M. Feliu, A. Aldaz, J. Electroanal. Chem. 243 (1988) 419.
[44] A. Crown, A. Wieckowski, J. Phys. Chem. Chem. Phys. 3 (2001) 3290.
[45] K.A. Friedrich, K.-P. Geyzers, A. Marmann, U. Stimming, R. Vogel, Z. Phys. Chem. 208S (1999) 137.
[46] S.R. Brankovic, J. McBreen, R.R. Adžić, Surf. Sci. 479 (2001) L363.
[47] T.J. Schmith, H.A. Gasteiger, G.D. Stäb, P.M. Urban, D.M. Kolb, R.J. Behm, J. Electrochem. Soc. 145 (1998) 2354.
[48] S.Lj. Gojkovic, S.K. Zecevic, R.F. Savinel, J. Electrochem. Soc. 145 (1998) 3713.

[49] K. Kinoshita, in: J.O'M. Bockris, B.E. Conway, R.E. White (Eds.), Modern Aspects of Electrochemistry, vol. 14, Plenum, New York, 1982.
[50] R.E. Benfield, J. Chem. Soc. Faraday Trans. 88 (1992) 1107.
[51] S.R. Brankovic, J.X. Wang, R.R. Adžić, Electrochem. Solid-State Lett. 4 (2001) A217.
[52] P. Waszczuk, J. Solla, H.-S. Kim, Y.Y. Tong, A. Aldaz, A. Wieckowski, J. Catal. Priority Commun. 203 (2001) 1.
[53] W.F. Lin, T. Iwasita, W. Vielsich, J. Phys. Chem. 103 (1999) 3250.
[54] Y. Ishikawa, M.-S. Liao, C.R. Cabrera, Surf. Sci. 463 (2000) 66.
[55] F. Buatier de Mongeot, M. Scherer, B. Gleich, E. Kopatzki, R.J. Behm, Surf. Sci. 411 (1998) 249.
[56] M.T.M. Koper, T.E. Shubina, R.A. van Santen, J. Phys. Chem. 106 (2002) 689.
[57] B. Hammer, J.K. Nørskov, Adv. Catal. 45 (2000) 71.